





Controlling the Motion of Interfaces in Capillary Channels with Non-uniform Surface Wettability

Yüzey Islanabilirliği Üniform Olmayan Kılcal Kanallardaki Arayüzeylerin Hareketinin Kontrolü

Mehmet Alptuğ Boylu ¹, Umut Ceyhan ^{2*}

¹ Graduate School of Natural and Applied Sciences, İzmir Kâtip Çelebi University, 35620, İzmir, Türkiye

² Department of Mechanical Engineering, İzmir Kâtip Çelebi University, 35620, İzmir, Türkiye

Sorumlu Yazar / Corresponding Author *: umut.ceyhan@ikcu.edu.tr

Geliş Tarihi / Received: 17.12.2022

Kabul Tarihi / Accepted: 02.03.2023

Atıf şekli/ How to cite: BOYLU, M.A., CEYHAN, U.(2023). Controlling the Motion of Interfaces in Capillary Channels with Non-uniform Surface Wettability.DEUFMD, 25(75), 675-691.

Araştırma Makalesi/Research Article

DOI:10.21205/deufmd.2023257513

Abstract

The use of self-driven flows in microfluidic devices attracts many researchers as the external flow-driving mechanism is diminished or eliminated. One of the mechanisms providing such motions is generating a pressure difference across interfaces as in the case of the motion in capillary tubes. The capillarity, namely, the pressure difference across the interface due to its curvature drives the motion. This pressure depends on the interaction with the capillary walls and is controlled if one varies the surface energy of the walls. In this study, we search for the effects of surface energy on the motion of interfaces in capillary-driven flows. To this end, we model the motion of fluid particles in a capillary channel and integrate the governing equations using the binary lattice Boltzmann Method for the two-phase flow. We first validate our solver for canonical static and dynamic problems. We then discuss two main contributions; we show how to deviate the interface speed from the ones moving in channels with uniform wall energies and discuss the conditions under which such an interface stagnates (like a passive valve in a channel). Tuning the wettability of the channel walls, we provide a simple condition for stopping the interface: the summation of the equilibrium contact angles interface make with the channel walls at the bottom and top wall need to satisfy $\theta_{eq}^{bot} + \theta_{eq}^{top} \geq \pi$. Configurations and wetting properties of different wettability regions play major roles together.

Keywords: Capillarity, Wetting, Interfaces, Microfluidics, Lattice Boltzmann Method

Öz

Mikroakışkan cihazlarda kendinden tahrikli akışların kullanımı, harici akış tahrik mekanizması azaltıldığı veya ortadan kaldırıldığı için birçok araştırmacının ilgisini çekmektedir. Bu tür hareketleri sağlayan mekanizmalardan biri de, kılcal borulardaki harekette olduğu gibi, arayüzeyler arasında bir basınç farkı oluşturmaktır. Kılcallık, yani kanal boyunca arayüzey eğriliği nedeniyle oluşan basınç farkı, hareketi yönlendirir. Bu basınç kılcal duvarlarla etkileşime bağlıdır ve duvarların yüzey enerjisi değiştirilerek kontrol edilebilir. Bu çalışmada, yüzey enerjisinin kılcal tahrikli akıştaki arayüzeylerin hareketi üzerindeki etkileri araştırılmaktadır. Bu amaçla, bir kılcal kanaldaki sıvı parçacıklarının hareketi modellenmekte ve iki fazlı akış için ikili Lattice Boltzmann yöntemi kullanılmaktadır. Öncelikle standart statik ve dinamik problemler için çözücü doğrulanmaktadır. Sonrasında iki ana katkı tartışılmakta; arayüzey hızının, tekdüze duvar enerjilerine sahip kanallarda hareket edenlerden

nasıl saptırılacağı gösterilmekte ve böyle bir arayüzeyin durdurulduğu koşullar (bir kanaldaki pasif valf gibi) tartışılmaktadır. Kanal duvarlarının ıslanabilirliğini ayarlayarak, arayüzeyi durdurmak için basit bir koşul sağlanmaktadır: Arayüzeyin alt ve üst duvardaki kanal duvarlarıyla yaptığı denge temas açılarının toplamı $\theta_{eq}^{bot} + \theta_{eq}^{top} \geq \pi$ 'yi karşılamalıdır. Farklı ıslanabilirlik bölgelerinin konfigürasyonları ve ıslanma özellikleri birlikte önemli rol oynamaktadır.

Anahtar Kelimeler: Kapilarite, İslatma, Arayüzey, Mikroakışkanlar, Lattice Boltzmann Metodu

Nomenclature

a	Constant coefficient in Landau model	n_y	Number of lattices along y -axis
Ca	Capillary number ($\eta v / \gamma$)	\emptyset	Order parameter (phase field)
ε	Parameter for wetting property	$P_{\alpha\beta}$	Pressure tensor
η	Dynamic viscosity	p_g	Gas pressure
F_i	Body (external) force	p_l	Liquid pressure
f_i	Distribution function f	r	Radius of curvature
g_i	Distribution function g	ρ	Density
γ	Surface tension between fluids	S	Bounding surface of the corresponding ϑ
Γ	Constant of mobility	t	Time
h	Channel gap thickness	τ_α	Relaxation time parameter for fluid 1
κ	Coefficient in Landau model	τ_β	Relaxation time parameter for fluid 2
l	Capillary filling length	θ	Contact angle
λ	Viscosity ratio of fluids	θ_{eq}	Equilibrium contact angle
M	Mobility	v	Velocity
μ	Chemical potential	v_g	Kinematic viscosity of gas
\mathbf{n}	Outward unit normal	v_l	Kinematic viscosity of liquid
n_x	Number of lattices along x -axis	ϑ	Volume

1. Introduction

Interface motion in capillary-driven flows and wetting phenomena on heterogeneous substrates are observed in nature [1], mostly in plants-trees [2], lotus leaves [3], desert beetles [4], and butterfly wings [5], etc; and in engineering applications such as lab-on-chips [6-8], oil recovery [9], painting, and inkjet printing [10-12]. Understanding and controlling the motion of such interfaces are important in microfluidic devices. Generally, the interfaces are controlled with active methods (actuators, valves), which require labor and are not scalable, autonomous, and easy to adapt and implement [13,14]. We, instead, investigate the use of different wettability regions, e.g. provided by chemical heterogeneity in the control of interfaces passively which has plenty of advantages [15,16].

When an interface meets a solid surface, it makes a certain angle with the interface which is called contact angle. This angle depends on the nature of the solid surface and the history of how the interface is established. For atomically smooth and chemically homogeneous surfaces, this angle is unique [17]. However, in nature, there are always heterogeneities or the surface can be designed as heterogeneous on purpose [18]. In this case, the contact angle is not unique; there is contact angle hysteresis (CAH) [19-21]. The heterogeneities, either physical or chemical, may cause contact line pinning/depinning. Because the spreading droplets over rough substrates and evaporation/condensation of droplets cause a natural motion of interfaces, the CAH over heterogeneous surfaces for such interfaces takes the great attention of many researchers [22-24]. The capillaries also provide such motion for the interfaces. For a liquid filling a capillary, the

motion of the interface is driven only by the pressure difference across the liquid interface. With the advancement in the understanding of wetting phenomena, its use in microfluidic devices has been increasing.

The physics of fluids at micron-scale is affected by the surface energy of the interfaces, here, the strong interaction between the fluid and solid substrate [25,26]. The motion of the contact line where the liquid meets the solid surface is dominated by viscous and surface tension forces rather than inertial and gravitational forces [27,28]. The ratio of the two is the Capillary number. Any change in the chemical structure of the surface over which the contact line moves changes the dynamics of the contact line motion. We discuss, in this study, the control of interface motion within a capillary, driven by capillary pressure, with the chemically structured walls.

We solve hydrodynamic equations to model the interface motion in a capillary with lattice Boltzmann Method. Navier-Stokes, continuity, and phase-field equations are modified into lattice Boltzmann equation using Chapman Enskog expansion in the limit of long length and time scales [29]. Besides, like the structural heterogeneities [30,31], similar effects are observable with chemical heterogeneities [17,32-34]. To do so, we model the motion of interfaces with lattice Boltzmann Method (LBM) and discuss the effects of chemical heterogeneity on the interface motion.

In the paper's following sections, we begin by introducing the method that we use to simulate capillary problems. We summarize different implementations for the method as Bhatnagar-Gross-Krook (BGK), Multiple Relaxation Time (MRT), etc. [35]. After the methodology, we present validations of our solver for static (Young equation) and dynamic (Washburn's and Cox-Voinov laws) problems. Later, we discuss the effect of chemical heterogeneity on the interface motion within capillaries.

2. Methodology

2.1. Governing equations

In the continuum regime, the motion of fluid particles within the capillary is governed by the Navier-Stokes equations of motion and the continuity for Newtonian fluid and given by equations (1) and (2) in index notation, respectively.

$$\partial_i(\rho v_i) + \partial_j(\rho v_j v_i) = -\partial_j P_{ji} + \partial_j(\eta(\partial_i v_j + \partial_j v_i)) + \rho F_i \quad (1)$$

$$\partial_i \rho + \partial_j(\rho v_j) = 0 \quad (2)$$

where ρ is the density, η is the dynamic viscosity of the fluid, and v_j is the fluid velocity. In equations (1) and (2), the indices i, j vary from 1 to 2 in two-dimensional problem and twice appearing index j in an expression means summation over it. On the right-hand-side of equation (1), the second term corresponds to the viscous forces, the third term is the external body force per unit volume. The first term includes the pressure tensor P_{ji} defined as

$$P_{ji} = \left(p_0 - \kappa \nabla^2 \phi - \frac{\kappa}{2} |\nabla \phi|^2 \right) \delta_{ji} + \kappa \partial_j \phi \partial_i \phi. \quad (3)$$

Inside the pressure tensor, there are pressure forces and surface tension forces, ϕ is an order parameter that comes from the Landau Free Energy to be defined shortly. The bulk pressure in equation (3) is defined as

$$p_0 = \frac{c^3}{3} \rho + a \left(-\frac{1}{2} \phi^2 + \frac{3}{4} \phi^4 \right). \quad (4)$$

We couple interface profile and fluid motion with pressure as follows [36]. For non-uniform composition, $-\nabla \mu$ models the surface tension forces which come from the divergence of P_{ji} and it acts locally in the fluid (chemical potential provides the opposite motion of the two phases defined as $\pm \phi$).

$$\nabla \mu = \partial_j P_{ji}, \quad (5)$$

and the phase field is governed by a Cahn-Hilliard type equation [37,38]

$$\partial_t \phi + \partial_j(\phi v_j) = M \nabla^2 \mu. \quad (6)$$

In equation (6), M is termed as mobility which controls the strength of the diffusion. The phase field ϕ responds to gradients by diffusion (as given on the right-hand-side); and, it also varies in time as it is convected by v_j (as given on the left-hand-side).

2.2. Thermodynamics of the fluid: modelling free energy

We use Landau theory to describe the binary fluids' free energy. It uses ϕ as an order parameter. Landau free energy is defined as

$$F = \int \left(\varphi(\phi) + \frac{\kappa}{2} |\nabla\phi|^2 \right) d\vartheta + \int (\varepsilon\phi) dS \quad (7)$$

where ϑ is the volume and S is the bounding surface of the corresponding volume, and the bulk free energy density $\varphi(\phi)$ is

$$\varphi(\phi) = \frac{c^2}{3} \rho \ln \rho + a \left(-\frac{1}{2} \phi^2 + \frac{1}{4} \phi^4 \right). \quad (8)$$

We take ρ as fluid density and ϕ as the order parameter, or phase field, $\phi = \pm 1$ defines different fluids; c can be written as $\frac{\Delta x}{\Delta t}$ (Δx spacing between the points or lattices and Δt time step) and a is a constant. The κ term in equation (7) defines the surface tension of the interfaces by penalizing non-uniformities (penalizes sharp gradients) in ϕ . Surface tension between the phases can be computed with $\gamma_{lv} = \sqrt{8\kappa a/9}$ [39].

While the first terms describe a second-order phase transition in the Landau function, the second integral in equation (7) defines the solid-fluid interactions and models the surface tension between them. We control the contact angle with the ε parameter. For controlling the contact angle, we take partial derivative for ϕ at the boundary, with respect to the normal of the surface $\partial_{\perp} \phi|_w = \varepsilon/\kappa$.

We show the order parameter in Figure 1 with the minimum points defining the equilibrium state at fixed volume and temperature, equilibrium states are given by global minima of the free energy, F . The variation of equation (7) with respect to ϕ , on the other hand, defines the chemical potential which is constant in equilibrium as

$$\mu = \frac{\delta F}{\delta \phi} = a(-\phi + \phi^3) - \kappa \nabla^2 \phi. \quad (9)$$

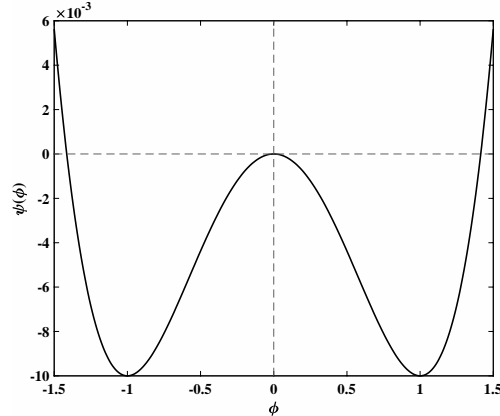


Figure 1. Phase separation, equilibrium values at $\pm\phi$.

Şekil 1. Faz ayrımı, $\pm\phi$ 'da denge değerleri.

For the numerical solution of the governing equations, we use lattice Boltzmann Method. Applying Chapman-Enskog expansion [29] shows that the lattice Boltzmann method recovers the hydrodynamic (governing) equations.

2.3. Lattice Boltzmann implementation

We solve the hydrodynamic equations stated in equations (1) and (2) with lattice Boltzmann method.

For the rest of the study, the dimensions are given in lattice units. As we analyze the physical behavior of interfaces for a binary fluid system, we use two distribution functions as $f_i(r, t)$ and $g_i(r, t)$. The subscript i shows the directions defined in a vector e_i , that the lattice point can travel. The values are as follows: $e_0 = (0,0), e_1 = (+c, 0), e_2 = (-c, 0), e_3 = (0, +c), e_4 = (0, -c), e_5 = (+c, +c), e_6 = (-c, -c), e_7 = (-c, +c), e_8 = (+c, -c)$. The physical quantities can be constructed from the distribution functions by

$$\rho = \sum_i f_i, \phi = \sum_i g_i, \rho v = \sum_i f_i e_i. \quad (10)$$

In LBM, we separate the collision (equations (11-12)) and streaming (equations (13-14)) operations [40] as given by

$$f'_i(r, t) = f_i(r, t) - inv[M] \left(S(M[f_i - f_i^{eq}]) \right), \quad (11)$$

$$g'_i(r, t) = g_i(r, t) - \frac{1}{\tau_\phi} [g_i - g_i^{eq}], \quad (12)$$

$$f_i(r + e_i \Delta t, t + \Delta t) = f'_i(r, t), \quad (13)$$

$$g_i(r + e_i \Delta t, t + \Delta t) = g'_i(r, t). \quad (14)$$

For the collision part, there is a collision operator parameter which includes a time constant τ as "relaxation time" parameter and describes the speed of the system to reach its equilibrium. The viscosity and heat diffusivity are affected by the relaxation time. Actually, Boltzmann's original collision operator is non-trivial. It includes all the possibilities for a collision of two particles. However, there is a simple operator that directly captures the relaxation of the distribution function using single relaxation time (SRT) τ , to its equilibrium. Bhatnagar, Gross and Krook (BGK) collision operator [41] is given by

$$\Omega(f) = -\frac{1}{\tau} (f - f^{eq}). \quad (15)$$

Though the BGK operator is simple and efficient, it has lower accuracy and stability problems compared to Two-Relaxation-Time and Multiple-Relaxation-Time operators. We implement Multiple-Relaxation-Time (MRT) operator because it consists of more than two free parameters (relaxation times) to be arranged for more stable and accurate results.

In the BGK operator, we define only one relaxation parameter for the Boltzmann equation; but, in the multiple relaxation time, we define multiple relaxation parameters inside S matrix, M matrix and its inverse [42].

The equilibrium distribution functions can be shown as f_i^{eq} and g_i^{eq} . The relations between f_i and g_i is provided with f_i^{eq} and g_i^{eq} . We choose the equilibrium functions and gradients in a way to reduce spurious velocities around the interfaces [43].

The relaxation parameters seen in equation (12) and in matrix S in equation (11) are τ_ρ and τ_ϕ . While the τ_ϕ is fixed and unity, τ_ρ varies from one lattice node to another by

$$\tau_\rho = \tau_\beta + \frac{\phi + 1}{2} (\tau_\alpha - \tau_\beta) \quad (16)$$

where τ_α and τ_β are the relaxation parameters that describe the fluids' viscosities. These

relaxation parameters are related to the kinematic viscosity and mobility as

$$\nu = \Delta t \frac{c^2}{3} \left(\tau_\rho - \frac{1}{2} \right), \quad (17)$$

$$M = \Delta t \Gamma \left(\tau_\phi - \frac{1}{2} \right) \quad (18)$$

where Γ is a parameter that we set in the equilibrium to change mobility.

Finally, we use the halfway bounce-back method [44] ($f_i(x_N, t + \Delta t) = f_{opp(i)}^*(x_N, t)$) to apply no-slip boundary condition on the walls and use periodic boundary conditions as needed within the streaming step.

3. Interfaces with Chemically Homogeneous Surfaces: Validation

We devote this section to interfaces meeting chemically homogeneous surfaces for validation purposes. The capability of our solver for an interface to attain the correct equilibrium angle (static angle) is crucial for the moving interfaces. We first validate our solver for static wetting problems on chemically homogeneous substrates for different surface energies. We measure the contact angles of certain droplet-substrate combinations to compare with the Young value. Second, we analyze the motion of interfaces within a capillary.

3.1. Static validation

When a droplet meets a clean surface and remains in hydrostatic equilibrium, the contact angle it makes with the surface is given by the Young [45] value as

$$\cos \theta_{eq} = \frac{\gamma_{sv} - \gamma_{sl}}{\gamma_{lv}} \quad (19)$$

where γ_{sv} , γ_{sl} and γ_{lv} are the surface tensions between solid-vapor, solid-liquid and liquid-vapor interfaces, respectively.

For a given liquid with fixed γ_{lv} , we vary the surface energy by tuning the normal gradient of ϕ at the boundary and setting the equilibrium contact angle given by

$$\sqrt{\frac{2\kappa}{a}} \partial_\perp \phi|_w = 2 \operatorname{sgn} \left(\theta_{eq} - \frac{\pi}{2} \right) \times \left[\cos \left(\frac{\theta}{3} \right) \left(1 - \cos \left(\frac{\theta}{3} \right) \right) \right]^{\frac{1}{2}} \quad (20)$$

where $\theta = \arccos((\sin \theta_{eq})^2)$ [39].

We place a droplet on a flat substrate that is atomically smooth and chemically homogeneous. No external forces are acting on

the droplets and the surface tension is treated to be uniform. We initialize the droplets as a semicircle and let them converge to their equilibrium shape.

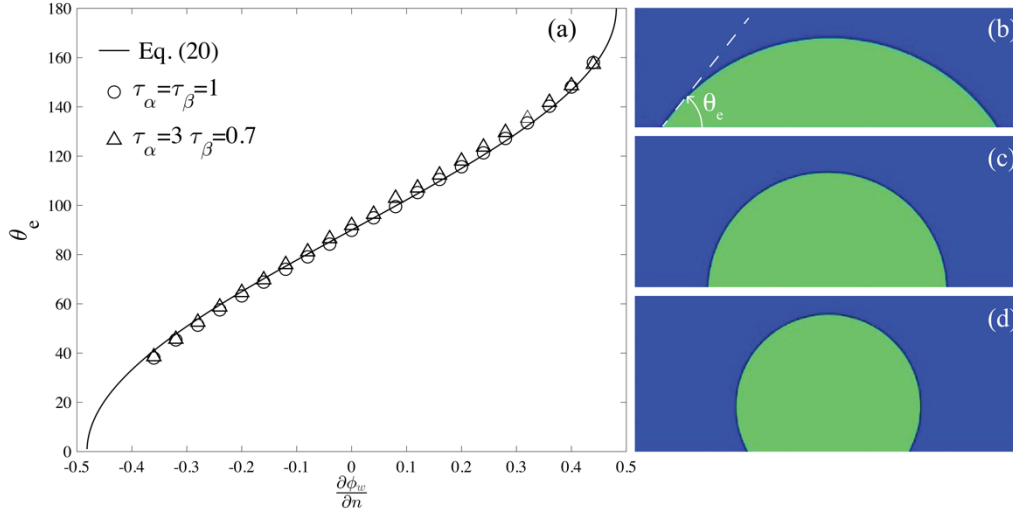


Figure 2. (a) The variation of equilibrium contact angle with gradient of ϕ at the wall, $\partial_\perp \phi|_w$, for the same and different viscosities, respectively. Circles and triangles are simulation results obtained using MRT lattice Boltzmann. We show the theoretical expression given in equation 20 with a solid line. (b), (c) and (d) show the equilibrium shapes of the droplets with 60°, 90° and 120° respectively.

Şekil 2. (a) Sırasıyla aynı ve farklı viskoziteler için denge temas açısının duvardaki ϕ gradyanı $\partial_\perp \phi|_w$ ile değişimi. Daireler ve üçgenler, MRT lattice Boltzmann kullanılarak elde edilen simülasyon sonuçlarıdır. Denklem 20’de verilen teorik ifadeyi düz bir çizgi ile gösteriyoruz. (b), (c) ve (d) sırasıyla 60°, 90° ve 120° ile damlacıkların denge şekillerini göstermektedir.

In Figure 2(a), we compare the computed equilibrium contact angles with equation (20) and show the interface profiles for both partial wetting and non-wetting cases through Figure 2(b)-(d). We perform the contact angle measurement by fitting a circle to the interface which is defined at the transition of ϕ from -1 to 1 . The theory and computation match for the range of contact angles studied using MRT lattice Boltzmann method for both equal and different viscosity fluids. Using BGK instead of MRT ends up with a deviation from the theory for different viscosities. A similar observation can be seen in C.M. Pooley *et al.* [42].

3.2. Dynamic validation

Capillary filling is one of the examples of moving contact line problems due to pressure difference across the moving interface. Because the motion does not require an external driving mechanism, it is one of the promising methods used in microfluidics. Washburn [46] defines the filling of a smooth capillary with constant surface

energy. By neglecting the inertial effects, end effects and viscous effects due to displaced fluid (e.g. gas) by the filling liquid, the motion of the penetrating incompressible liquid is defined by Poiseuille flow. The position, z , of the interface as a function of time can be shown to obey the following power law relation

$$z(t)^2 - z_0^2 = l(t)^2 = \left(\frac{\gamma_{lv} h \cos \theta(t)}{3\eta} \right) t \quad (21)$$

with $z(t = 0) = z_0$ and l being the filling length. The dynamic viscosity of the liquid is η , the channel gap thickness is h and θ is the contact angle the liquid makes with the channel walls.

When the viscosity of the displaced fluid is comparable to the fluid viscosity filling the capillary, we use the modified version of Washburn's equation. In equation (22), both viscosities affect the filling (in equation (21), the small one is neglected).

$$\eta_\alpha \frac{l(t)^2}{2} + \eta_\beta \left(Ll(t) - \frac{l(t)^2}{2} \right) = \left(\frac{\gamma_{lv} h \cos \theta(t)}{6} \right) (t + t_0) \quad (22)$$

For fluids having the same viscosity, equation (22) reduces to equation (23).

$$l(t) = \left(\frac{\gamma_{lv} h \cos \theta(t)}{6 \eta_\alpha L} \right) (t + t_0) \quad (23)$$

In equations (22) and (23), t_0 is the integration constant which can be adjusted depending on the initial position of the interface. It is zero if $l(0)=0$. While equation (23) scales linearly with time, equation (22) scales as $\frac{1}{2}$ power of time.

In Figure 3, we show the problem setup. The channel walls of length L are shown in black. The periodic inlet and outlet boundaries ensure mass

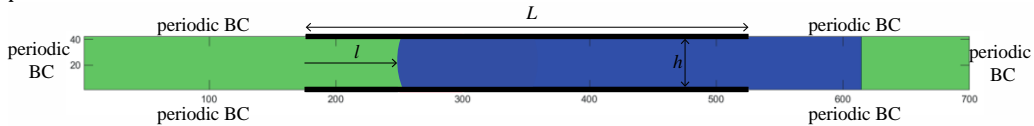


Figure 3. Capillary filling problem setup. The wall length is L , the green fluid is liquid and the other one is gas. Filling length (l) is the distance that liquid penetrates into the capillary tube. For the rest of the study, the contact angle on black-colored regions on capillary walls is equal to $\theta_{eq} = 60^\circ$.

Şekil 3. Kılcal dolma problem düzeneği. Duvar uzunluğu L , yeşil akışkan sıvı ve diğeri gazdır. Doldurma uzunluğu (l), sıvının kılcal boruya girdiği mesafedir. Çalışmanın geri kalanı için kılcal duvarlardaki siyah renkli bölgelerdeki temas açısı $\theta_{eq} = 60^\circ$ 'ye eşittir.

The differences are, where we observe deviations from initial conditions, Poiseuille flow profile and inertial effects. In Figure 4(a), solid lines come from modified Washburn's equation [33] and dashed lines are theoretical values with a refinement of $l^{eff} = l + H/2$. So, we add imaginary walls with a length of $H/2$ at both ends of the capillary tube to get rid of inlet/outlet effects. A similar approach can be seen in Pooley *et al.*[43]. The filling length data form straight lines because the viscous dissipation occurs in capillary at the same rate. So we observe, it is independent of the interface position. As shown in Figure 4(b), after the interface passes the beginning of the capillary, the results agree with Washburn's equation. For the filling distances at a certain time, as we expect, the interface moves faster for lower wetting angles.

Because the capillary-driven flow is a contact line motion problem, we also validate if the dynamic contact angles satisfy the Cox-Voinov [47,48] relation which states there is a linear

conservation while the top and bottom periodic sides provide us with a flat interface mimicking infinite reservoirs at both ends. All dimensions are given in lattice units.

We use $N_x = 700$ and $N_y = 42$ lattices along x and y -directions, respectively; and place the capillary walls in the middle of the domain at the top and bottom. We set $\kappa = 0.04$, $a = 0.04$ and $M = 1$ in the MRT lattice Boltzmann implementation. For different viscosity cases, we set the kinematic viscosities to $\nu_l = 0.83$ and $\nu_g = 0.067$ (this corresponds to $\tau_\alpha = 3$, $\tau_\beta = 0.7$ as in [43] with viscosity ratio of $\lambda = 12.4$).

relationship between the cube of dynamic contact angle and the Capillary number.

We show in Figure 5 this linear variation of Ca with the cube of the dynamic contact angle for four different surface energies. Considering each individual case, as the viscosities of the filling and displaced liquids are different, the contact angle of the filling liquid decreases with time and as a result, the speed of the filling slows down [49]. But if we compare all cases for different contact angles, the speed of the capillary increases with increasing wettability (with lower θ_{eq}) as shown in Figure 4.

For comparison, see the mean velocities (using Ca values above) for different wettabilities with constant viscosity and surface tension in Figure 6. Apart from these validations, we compare the velocity of the interface with the one given in Figure 6 of C.M. Pooley and Yeomans [43] and it matches well.

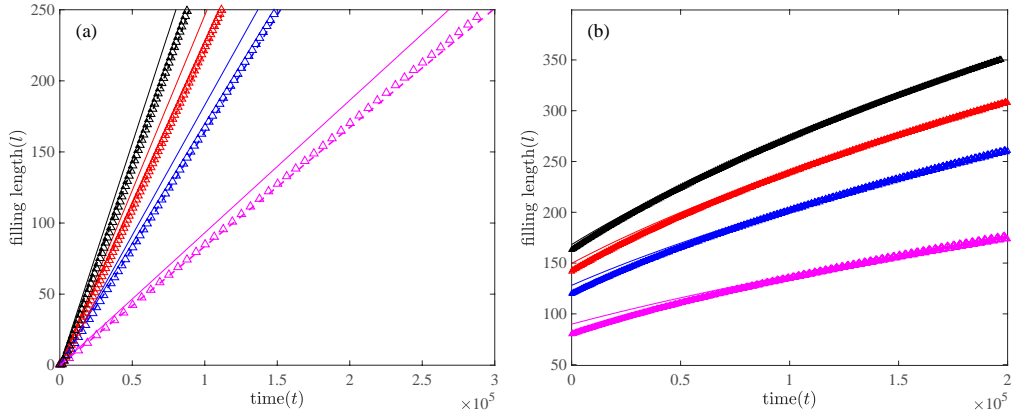


Figure 4. The simulation result of filling length as a function of time, comparison with Washburn's equation for same (a) and different (b) viscosities. Magenta color is used for $\theta_{eq} = 75^\circ$, blues for $\theta_{eq} = 60^\circ$, reds for $\theta_{eq} = 45^\circ$ and blacks for $\theta_{eq} = 30^\circ$. The symbols are our computations, the solid lines in (a) are modified theoretical values for the same viscosity fluid flow (equation (23)) and in (b) are theoretical values for different viscosity fluid flow (equation (21)) which are calculated with dynamic angles. The dashed lines in (a) are corrected values for the same viscosity cases.

Şekil 4. Doldurma uzunluğunun zamanın bir fonksiyonu olarak simülasyon sonucu, aynı (a) ve farklı (b) viskoziteler için Washburn denklemiyle karşılaştırma. $\theta_{eq} = 75^\circ$ için macenta, $\theta_{eq} = 60^\circ$ için mavi, $\theta_{eq} = 45^\circ$ için kırmızı ve $\theta_{eq} = 30^\circ$ için siyah kullanılmıştır. Semboller bizim hesaplamalarımızdır, (a)'daki kesintisiz çizgiler aynı viskoziteli sıvı akışı (denklem (23)) için değiştirilmiş teorik değerlerdir ve (b)'deki farklı viskoziteli sıvı akışı (denklem (21)) için teorik değerlerdir; dinamik açılarla hesaplanmıştır. (a)'daki kesikli çizgiler, aynı viskozite durumları için düzeltilmiş değerlerdir.

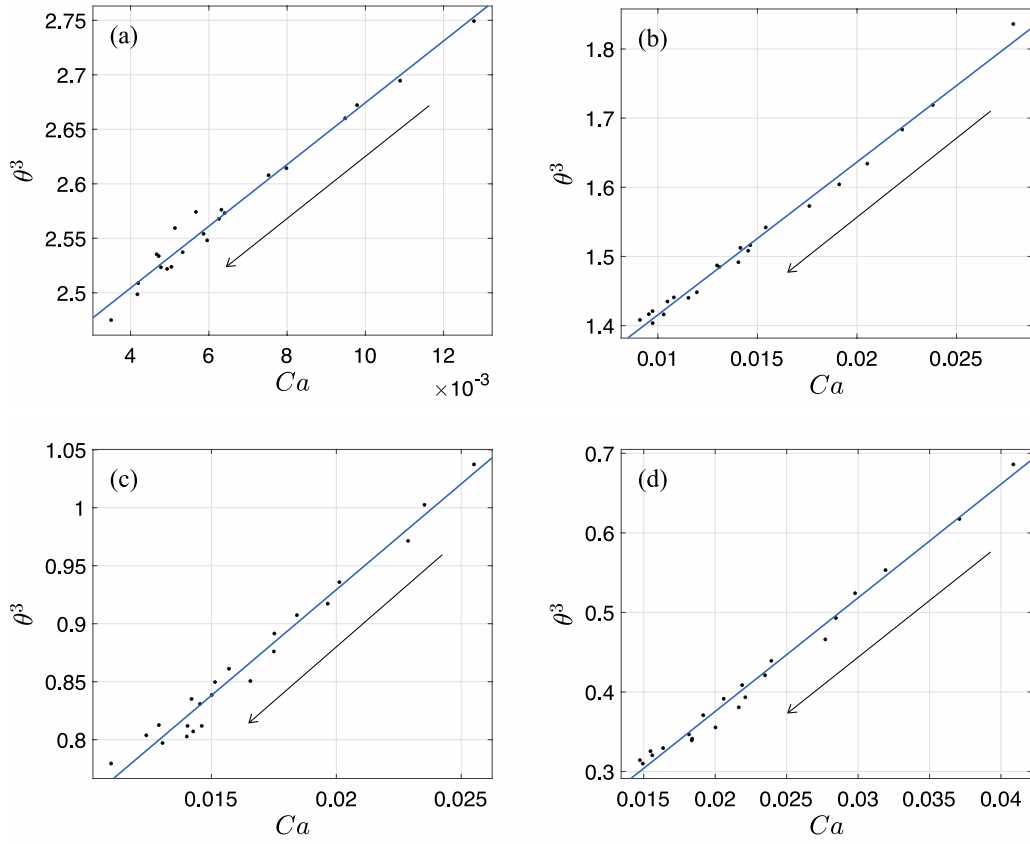


Figure 5. Variation of dynamic contact angle with Ca , (a) $\theta_{eq} = 75^\circ$, (b) $\theta_{eq} = 60^\circ$, (c) $\theta_{eq} = 45^\circ$, (d) $\theta_{eq} = 30^\circ$, arrows show the filling direction.

Şekil 5. Dinamik temas açısının Ca ile değişimi, (a) $\theta_{eq} = 75^\circ$, (b) $\theta_{eq} = 60^\circ$, (c) $\theta_{eq} = 45^\circ$, (d) $\theta_{eq} = 30^\circ$, oklar dolun yönünü göstermektedir.

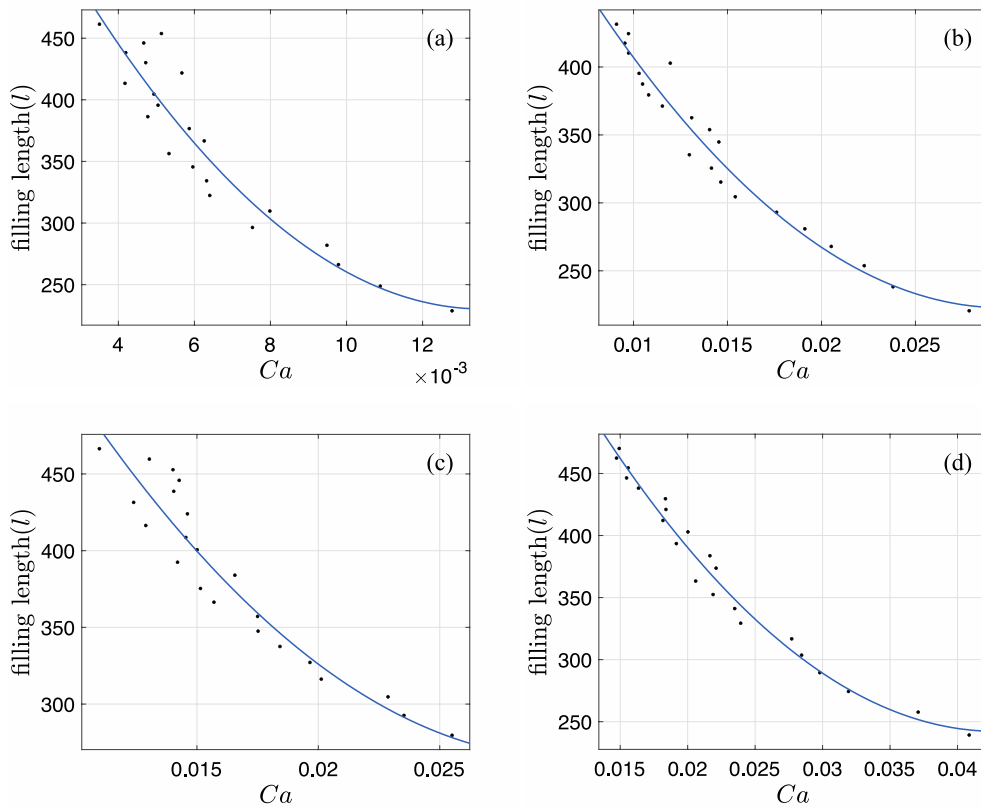


Figure 6. Filling length variation with Ca , (a) $\theta_{eq} = 75^\circ$, (b) $\theta_{eq} = 60^\circ$, (c) $\theta_{eq} = 45^\circ$, (d) $\theta_{eq} = 30^\circ$.

Şekil 6. Doldurma boyunun Ca ile değişimi, (a) $\theta_{eq} = 75^\circ$, (b) $\theta_{eq} = 60^\circ$, (c) $\theta_{eq} = 45^\circ$, (d) $\theta_{eq} = 30^\circ$.

4. Effect of Chemical Heterogeneity

The roughness and chemical heterogeneity are common features of surfaces except the ones manufactured in a laboratory as atomically smooth and chemically homogeneous. Inspired by nature, these features are mimicked to control the motion of interfaces. Among the various microfluidic devices, capillary-driven flows are popular as there is no need for an external driving mechanism. We study the motion of interfaces in a channel which is driven by capillarity. To slow down or stagnate the interface motion within some regions, we investigate the effects of varying wettability. This can be achieved using electrowetting [50-52] or the channels can be manufactured with chemically and/or physically heterogeneous patterns to pin/depin the interface as a passive control method. We mimic such a surface by chemical heterogeneities on the channel walls. By chemical heterogeneity we mean the energy

of the surface is not uniform, it is altered by modifying the surface chemistry rather than the topology. We achieve this numerically by adjusting the normal gradient of ϕ within the region of interest to achieve the desired θ_{eq} .

Using the channel geometry given in Figure 3; we first observe the deviation of the interface speed from Washburn's law when there is a chemical defect on the channel walls. To this end, we consider two cases: one with more ($\theta_{eq} = 30^\circ$) and one with less hydrophilic ($\theta_{eq} = 75^\circ$) region on the top wall than the rest of the channel walls which is set to $\theta_{eq} = 60^\circ$. We show this deviation for single defects in Figure 7(a) by plotting the time variation of the filling length. We set the length of the defect region to 20 lattices and the deviation from Washburn's law for $\theta_{eq} = 60^\circ$ everywhere is obvious. Within a more hydrophilic region, the contact line speeds up increasing the filling speed with an increase in

the slope until it passes this region and attains the regular slope (see squares). The opposite is true for a less hydrophilic defect. The contact line motion slows down within this region and attains the same speed after (see triangles). In panel (b) of the same figure, we show, this time, the deviation for single patterns on both top and bottom walls in overlapped and staggered configurations.

The slowing down of the interface motion is more effective if the patterns are placed in an overlapped configuration as the contact lines at the top and bottom walls slow down at the same time. In the staggered configuration, however, the slowing down is limited because one of the contact lines moves faster while the other one moves slower. We show this in Figure 8 by comparing the two configurations. This observation suggests that overlapped heterogeneities prevail over staggered ones to stop the motion of the interfaces.

With this motivation, we search for the equilibrium states of the interface; namely, the conditions which flatten the interface resulting

in no pressure difference across the interface to derive the motion so that interface stops. In plane, the existence of interface curvature drives the motion. Such a flat interface is possible, for example, if both top and bottom contact angles attain 90° . In Figure 9, we observe a vertical flat interface satisfying our claim. For the top and bottom defects, we set the surface energies for the liquid to have contact angles of 90° while the rest of the channel walls remain at 60° . Normal stress balance at a local point at the interface with uniform surface tension γ requires

$$p_l - p_g = \gamma \nabla \cdot \mathbf{n} \sim \frac{\gamma}{r} \quad (24)$$

where \mathbf{n} is the outward unit normal pointing from the liquid into the gas and r is the radius of the curvature of the interface approximated by a circular arc. For the flat case, r goes to infinity and the pressure difference across the interface vanishes. This mechanism stops the interface.

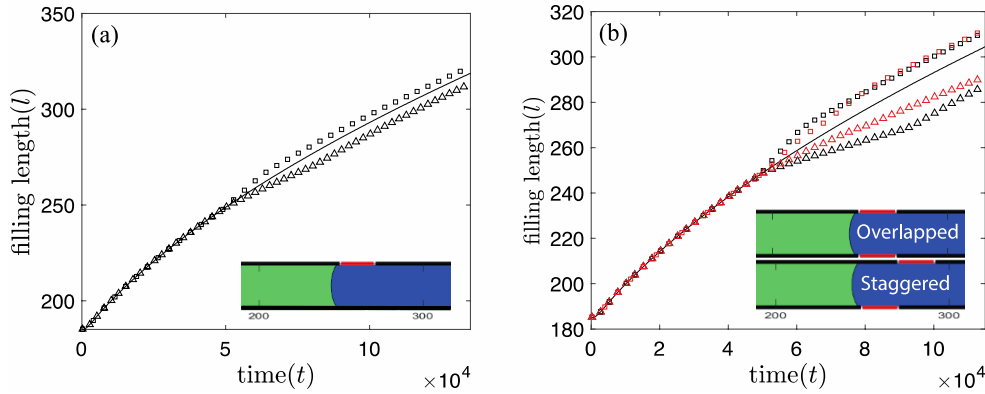


Figure 7. The divergence of filling length from Washburn for $\theta_{eq} = 60^\circ$, with (a) single defect on the capillary (squares for $\theta_{eq} = 30^\circ$ and triangles for $\theta_{eq} = 75^\circ$), (b) multi-defects on the capillary (black squares for overlapped $\theta_{eq} = 30^\circ$ regions, black triangles for overlapped $\theta_{eq} = 75^\circ$ regions, red squares for staggered $\theta_{eq} = 30^\circ$ regions and red triangles for staggered $\theta_{eq} = 75^\circ$ regions), to speed up or down the interface.

Şekil 7. Arayüzeyi hızlandırmak veya yavaşlatmak amacı ile doldurma uzunluğunun $\theta_{eq} = 60^\circ$ için Washburn'den sapması, (a) kılcal kanal üzerinde tek kusur ($\theta_{eq} = 30^\circ$ için kareler ve $\theta_{eq} = 75^\circ$ için üçgenler), (b) kılcal kanal üzerinde çoklu kusurlar (üst üste binen $\theta_{eq} = 30^\circ$ bölgeleri için siyah kareler, üst üste binen $\theta_{eq} = 75^\circ$ bölgeleri için siyah üçgenler, çakışmayacak şekilde ayarlanmış $\theta_{eq} = 30^\circ$ bölgeleri için kırmızı kareler ve çakışmayacak şekilde ayarlanmış $\theta_{eq} = 75^\circ$ bölgeleri için kırmızı üçgenler).

But if the regions are staggered not overlapped, then the filling of the capillary may not stop as seen in Figure 10. While panel (a) shows the deviation of interface position from uniform

surface energy surface, panels (b) to (e) show the corresponding interface profiles. The flow slows down but does not stop because $\theta_{eq}^{bot} + \theta_{eq}^{top} < 180^\circ$, it continues to move and only the interface

can be flat at the intersection of the regions for a small time interval. Therefore, at that point, the conditions are changed to $\theta_{eq}^{bot} + \theta_{eq}^{top} < 180^\circ$ and the interface again starts to move.

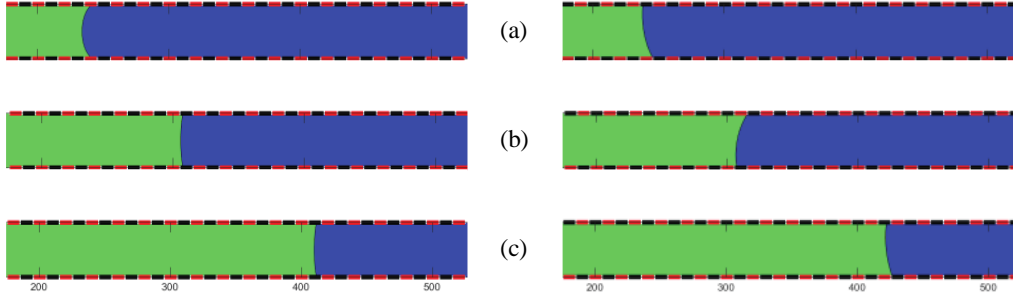


Figure 8. Comparison of the effect of wall pattern on the interface motion, the left panel is for the overlapped configuration while the right panel is for the staggered configuration, (a) $t = 50000$, (b) $t = 150000$, (c) $t = 400000$.

Şekil 8. Duvar deseninin arayüzey hareketi üzerindeki etkisinin karşılaştırılması, sol panel üst üste binen konfigürasyon içindir, sağ panel çakışmayacak şekilde ayarlanmış konfigürasyon içindir, (a) $t = 50000$, (b) $t = 150000$, (c) $t = 400000$.



Figure 9. Interface profile within the capillary at 90-degree regions.

Şekil 9. 90 derecelik bölgelerde kılcal kanal içindeki arayüzey profili.

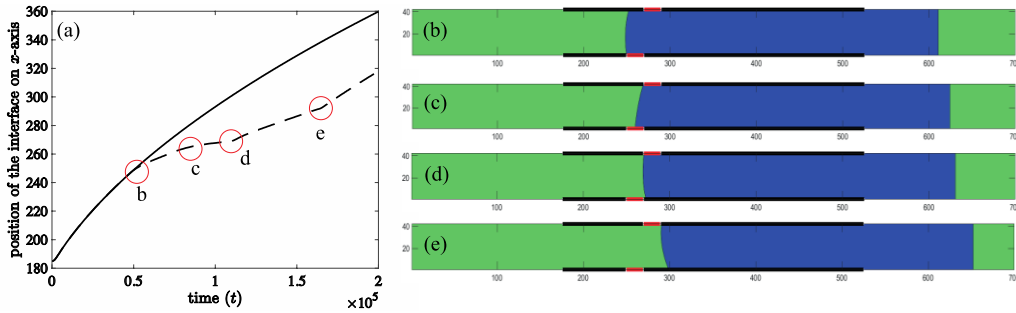


Figure 10. History of interface movement for staggered configuration with $\theta_{eq} = 90^\circ$ defects. The solid line in (a) shows the computed interface position for uniform $\theta_{eq} = 60^\circ$, dashed line is for staggered configuration. The interface shapes at several instants encircled in (a) are shown in panels (b) to (e).

Şekil 10. $\theta_{eq} = 90^\circ$ kusurlarla çakışmayacak şekilde ayarlanmış konfigürasyon için arayüzey hareketi geçmişi. (a)'daki kesintisiz çizgi, uniform $\theta_{eq} = 60^\circ$ için hesaplanan arayüzey konumunu gösterir, kesikli çizgi çakışmayacak şekilde ayarlanmış yapılandırma içindir. (a)'da daire içine alınmış çeşitli anlardaki arayüzey şekilleri, (b) - (e) panellerinde gösterilmektedir.

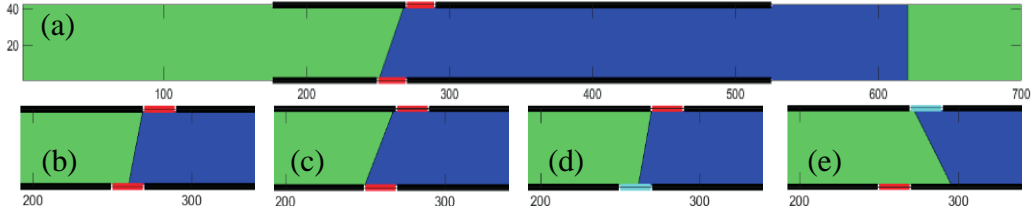


Figure 11. Various stopping cases, (a) case 1: Interface of the capillary at 120-degree regions with staggered configuration, (b) case 2, (c) case 3, (d) case 5, (e) case 6; see Table 1 for details.

Şekil 11. Çeşitli durma durumları, (a) durum 1: çakışmayacak şekilde ayarlanmış konfigürasyonla 120 derecelik bölgelerde kılcal kanal arayüzeyi, (b) durum 2, (c) durum 3, (d) durum 5, (e) durum 6; ayrıntılar için Tablo 1'e bakın.

In Figure 11, we see the stopping condition is provided only if $\theta_{eq}^{bot} + \theta_{eq}^{top} \geq 180^\circ$. This means that the flat interface does not have to be vertical. As long as, at any point in time, the contact angles at the top and bottom walls sum up to π , the interface could be stopped even for staggered configurations with hydrophobic regions.

The use of more hydrophobic regions for overlapped configurations does not affect the stopping mechanism, namely a vertical interface forms. But for the staggered configuration, more hydrophobic regions stop the interface at an inclined position as seen in Figure 11.

Table 1. Stopping conditions using the same setup as in Figure 11 for different wettability at defect regions. Except case 7 ($\theta_{eq} = 30^\circ$), all cases have $\theta_{eq} = 60^\circ$ out of the defects.

Tablo 1. Kusurlu bölgelerde farklı ıslanabilirlik için Şekil 11'deki ile aynı düzeneği kullanan durdurma koşulları. 7. durum ($\theta_{eq} = 30^\circ$) hariç, tüm durumlar kusurlar dışında $\theta_{eq} = 60^\circ$ 'ye sahiptir.

Parameters and Conditions \ Case Numbers	Case 1	Case 2	Case 3	Case 4	Case 5	Case 6	Case 7
$\theta_{eq}^{bot} & \theta_{eq}^{top}$	120&120	100&100	150&150	90&90	100&90	90&120	90&120
Vertically, $\theta_{eq}^{bot} + \theta_{eq}^{top} \geq 180^\circ$	Yes	No	Yes	No	No	2 nd region	No
Reaches 2 nd region?	No	Yes	No	Yes	Yes	Yes	Yes
Bottom-side contact angle (~%1)	112	100	113	-	100	60	-
Top-side contact angle (~%1)	68	80	67	-	80	120	-
Pinning at 1 st or 2 nd region?	First	Second	First	-	Second	Second	-
Stopping angle side	Top-side	Bottom-side	Top-side	-	Bottom-side	Bottom-side	-

As we summarize in Table 1, stopping conditions vary with the wettability of overlapped walls. We define a simple relation between the cases as;

1. If $\theta_{eq}^{bot} + \theta_{eq}^{top} \geq 180^\circ$, the interface stops and the contact line attains the θ_{eq} on the hydrophobic side.
2. Else, $\theta_{eq}^{bot} + \theta_{eq}^{top} < 180^\circ$, the interface moves but the contact line speed decreases. When the contact points are on walls that provide $\theta_{eq}^{bot} + \theta_{eq}^{top} \geq 180^\circ$, the interface starts to slow down. It tries to attain θ_{eq} for the side that has already depinned.

5. Conclusion

In this study, we analyze the interface motion in a capillary channel driven by capillary pressure only. Apart from the importance of such flows in microfluidic devices as it does not require an external device to drive the motion, it provides us with a flow domain to understand and control the interface motion. For this purpose, we modify the surface energy of the channel walls and investigate the passive control mechanism of interfaces instead of active methods.

We model the capillary flow as a two-phase flow of Newtonian fluids and integrate the governing equations using the lattice Boltzmann Method. This method has many advantages for wetting applications against traditional solvers such as Finite Element Method (FEM) compared to computing cost, applicability, mobility between cases, etc. We first validate our solver for static and dynamic problems and then discuss the effects of surface energy on the motion of interfaces.

We discuss two main problems: (i) Accelerating or decelerating the interfaces, (ii) interface stopping conditions. According to the cases of interface motion driven by capillarity, we can change the contact line speed and stop the interface as needed by playing with the energy of the surfaces. For changing the contact line speed, we add chemical defects on the walls which have different wettability properties. As we expect, according to the wettabilities of defects, deviation from the Washburn is observed, and for stopping conditions, we show that the defects should provide $\theta_{eq}^{bot} + \theta_{eq}^{top} \geq 180^\circ$ at the contact points of interface. The configurations of the defects can alter the stopping position of the interface.

We should, finally, note that if there are two interfaces in the capillary with uniform wall surface energy, the fluid column cannot move because the two interfaces are alike and cancel the pressure difference. However, it can be moved if the surfaces are modified to generate a wetting gradient that we are going to discuss in another paper.

We believe that our simulation would motivate further numerical and experimental studies for a possible setup including passively driven capillary flows to control the interface motion.

5. Sonuç

Bu çalışmada, sadece kılcal basınç tarafından yönlendirilen bir kılcal kanaldaki arayüzey hareketini inceliyoruz. Hareketi yönlendirmek için harici bir cihaz gerektirmediği için mikroakışkan cihazlarda bu tür akışların öneminin yanı sıra, arayüzey hareketini anlamak ve kontrol etmek için bize bir akış alanı sağlar. Bu amaçla kanal duvarlarının yüzey enerjisini modifiye ederek aktif yöntemler yerine arayüzeylerin pasif kontrol mekanizmasını araştırıyoruz.

Kılcal akışı Newtonyan sıvılarının iki fazlı akışı olarak modelliyoruz ve lattice Boltzmann Metodu'nu kullanarak yöneten denklemleri entegre ediyoruz. Bu yöntemin, ıslatma uygulamaları için Sonlu Elemanlar Yöntemi (FEM) gibi geleneksel çözücülere kıyasla hesaplama maliyeti, uygulanabilirlik, durumlar arasındaki hareketlilik vb. gibi birçok avantajı vardır. Önce çözücümüzü statik ve dinamik problemler için doğruluyoruz ve ardından arayüzeylerin hareketi üzerine yüzey enerjisinin etkilerini tartışıyoruz.

İki ana sorunu tartışıyoruz: (i) Arayüzeylerin hızlandırılması veya yavaşlatılması, (ii) arayüzeylerin durma koşulları. Kılcallık tarafından yönlendirilen arayüzey hareketi durumlarına göre, temas hattı hızını değiştirebilir ve yüzeylerin enerjisi ile oynayarak arayüzeyi gerektiği gibi durdurabiliriz. Temas hattı hızını değiştirmek için farklı ıslanabilirlik özelliklerine sahip duvarlara kimyasal kusurlar ekliyoruz. Beklediğimiz gibi, kusurların ıslanabilirliklerine göre Washburn'den sapma gözlenir ve durma koşulları için kusurların arayüzeyin temas noktalarında $\theta_{eq}^{bot} + \theta_{eq}^{top} \geq 180^\circ$ sağlaması gerektiğini gösteriyoruz. Kusurların konfigürasyonları arayüzeyin durma konumunu değiştirebilir.

Son olarak, kılcalda üniform duvar yüzey enerjisine sahip iki arayüzey varsa, sıvı kolonunun hareket edemeyeceğini, çünkü iki arayüzeyin aynı olduğunu ve basınç farkını iptal ettiğini not etmeliyiz. Ancak, başka bir yazıda tartışacağımız gibi bir ıslatma gradyanı oluşturularak yüzeyler değiştirilirse hareket sağlanabilir.

Simülasyonumuzun, arayüzey hareketini kontrol etmek amacı ile pasif olarak yönlendirilen kılcal akışlar içeren olası bir düzenek için daha fazla sayısal ve deneysel çalışmaları motive edeceğine inanıyoruz.

6. Statements of Ethical Approval and Conflict of Interest

The authors of this article declare that the methods used in this study do not require ethical approval. The authors also declare that they have no conflict of interest.

References

- [1] Darmanin, T. and Guittard, F., 2015. 'Superhydrophobic and superoleophobic properties in nature', *Materials Today* 18(5), 273–285. DOI: 10.1016/j.mattod.2015.01.001
- [2] Kohonen, M. M., 2006. 'Engineered wettability in tree capillaries', *Langmuir* 22, 3148–3153. DOI: 10.1021/la052861x
- [3] Barthlott, W., Neinhuis, C. 1997. 'Purity of the sacred lotus, or escape from contamination in biological surfaces', *Planta* 202, 1–8. DOI: 10.1007/s004250050096
- [4] Parker, A. R. and Lawrence, C. R., 2001. 'Water capture by a desert beetle', *Nature* 414, 33–34. DOI: 10.1038/35102108
- [5] Zheng, Y., Gao, X. and Jiang, L. 2007. 'Directional adhesion of superhydrophobic butterfly wings', *Soft Matter* 3, 178–182. DOI: 10.1039/B612667G
- [6] Yager, P., Edwards, T., Fu, E., Helton, K., Nelson, K., Tam, M.R., Weigl, B.H. 2006. 'Microfluidic diagnostic technologies for global public health', *Nature* 442, 412–418. DOI: 10.1038/nature05064
- [7] Sackmann, E.K., Fulton, A.L. and Beebe, D.J., 2014. 'The present and future role of microfluidics in biomedical research', *Nature* 507, 181–189. DOI: 10.1038/nature13118
- [8] Yeo, L.Y., Chang, H.C., Chan, P.P.Y., and Friend, J.R. 2011. 'Microfluidic devices for bioapplications', *Small* 7(1), 12–48. DOI: 10.1002/smll.201000946
- [9] Sonmez, I. and Cebeci, Y., 2004. 'Investigation of relationship between critical surface tension of wetting and oil agglomeration recovery of barite', *Colloids and Surfaces A: Physicochem. Eng. Aspects* 234, 27–33. DOI: 10.1016/j.colsurfa.2003.12.003
- [10] Dupuis, A. and Yeomans, J.M., 2004. Lattice Boltzmann modelling of droplets on chemically heterogeneous surfaces. *Future Generation Computer Systems*, 20(6), pp.993-1001. DOI: 10.1016/j.future.2003.12.012
- [11] Leopoldes, J., Dupuis, A., Bucknall, D.G. and Yeomans, J.M., 2003. 'Jetting micronscale droplets onto chemically heterogeneous surfaces', *Langmuir* 19, 9818–9822. DOI: 10.1021/la0353069
- [12] Verberg, R., Pooley, C.M., Yeomans, J.M. and Balazs, A.C., 2004. 'Pattern formation in binary fluids confined between rough, chemically heterogeneous surfaces', *Physical Review Letters* 93(18). DOI: 10.1103/PhysRevLett.93.184501
- [13] Au, A.K., Lai, H., Utela, B.R. and Folch, A., 2011. 'Microvalves and micropumps for biomems', *Micromachines* 2(2), 179–220. DOI: 10.3390/mi2020179
- [14] Hilber, W., 2016. 'Stimulus-active polymer actuators for next-generation microfluidic devices', *Applied Physics A* 122(751). DOI: 10.1007/s00339-016-0258-6
- [15] Arango, Y., Temiz, Y., Gökçe, O. and Delamarche, E., 2020. 'Electro-actuated valves and self-vented channels enable programmable flow control and monitoring in capillary-driven microfluidics', *Science Advances* 6(16). DOI: 10.1126/sciadv.aay8305
- [16] Mahmud, M. S., Alo, A., Farshchian, B., Lee, G.-H. and Kim, N., 2022. 'Pulsed laser ablation on polymethylmethacrylate (pmma) surfaces for capillary driven flows', *Surfaces and Interfaces* 31, 101989. DOI: 10.1016/j.surfin.2022.101989
- [17] Marmur, A., 1994a. 'Contact angle hysteresis on heterogeneous smooth

- surfaces', *J. Colloid Interface Sci.* 168(1), 40-46. DOI: 10.1006/jcis.1994.1391
- [18] Marmur, A., 1994b. 'Thermodynamic aspects of contact angle hysteresis', *Advances in Colloid and Interface Science* 50, 121-141. DOI: 10.1016/0001-8686(94)80028-6
- [19] Joanny, J.F. and De Gennes, P.G., 1984. 'A model for contact angle hysteresis', *J. Chem. Phys.* 81(552). DOI: 10.1063/1.447337
- [20] Adamson, A. W. and Gast, A. P., 1997. 'Physical chemistry of surfaces', A Wiley-Interscience Publication 6th Edition.
- [21] Sonmez, I. and Cebeci, Y., 2019. 'Contact angle hysteresis in a microchannel: Statics', *Physical Review Fluids* 4(044008). DOI: 10.1016/j.colsurfa.2003.12.003
- [22] Kusumaatmaja, H. and Yeomans, J.M., 2007. 'Modeling contact angle hysteresis on chemically patterned and superhydrophobic surfaces', *Langmuir* 23(11), 6019-6032. DOI: 10.1021/la063218t
- [23] Montes Ruiz-Cabello, F.J., Rodríguez-Valverde, M.A., Marmur, A. and Cabrerizo-Vílchez, M.A., 2011. 'Comparison of sessile drop and captive bubble methods on rough homogeneous surfaces: A numerical study', *Langmuir* 27(15), 9638-9643. DOI: 10.1021/la201248z
- [24] Chang, X., Huang, H., Lu, X.Y. and Hou, J., 2022. 'Width effect on contact angle hysteresis in a patterned heterogeneous microchannel', *J. Fluid Mech.* 949(A15). DOI: 10.1017/jfm.2022.763
- [25] Wang, X., Xu, B. and Chen, Z., 2020. 'Numerical simulation of droplet dynamics on chemically heterogeneous surfaces by lattice boltzmann method', *International Journal of Numerical Methods for Heat and Fluid Flow* 30(2), 607-624. DOI: 10.1108/HFF-03-2019-0259
- [26] Iwahara, D., Shinto, H., Miyahara, M. and Higashitani, K., 2003. 'Liquid drops on homogeneous and chemically heterogeneous surfaces: A two dimensional lattice boltzmann study', *Langmuir* 19, 9086-9093. DOI: 10.1021/la034456g
- [27] Tilehboni, S.M., Fattahi, E., Afrouzi, H.H. and Farhadi, M., 2015. 'Numerical simulation of droplet detachment from solid walls under gravity force using lattice boltzmann method', *Journal of Molecular Liquids* 212, 544-556. DOI: 10.1016/j.molliq.2015.10.007
- [28] Park, C.S., Baek, S.Y., Lee, K.J. and Kim, S.W., 2003. 'Two-phase flow in a gas-injected capillary tube', *Advances in Polymer Technology* 22(4), 320-328. DOI: 10.1002/adv.10059
- [29] Frisch, U., d'Humières, D., Hasslacher, B., Lallemand, P., Pomeau, Y. and Rivet, J.P., 2019. Lattice gas hydrodynamics in two and three dimensions. In *Lattice Gas Methods for Partial Differential Equations*. CRC Press, pp. 77-136.
- [30] Dutka, F., Napiórkowski, M. and Dietrich, S., 2012. 'Mesoscopic analysis of gibbs' criterion for sessile nanodroplets on trapezoidal substrates', *The Journal of Chemical Physics* 136(064702). DOI: 10.1063/1.3682775
- [31] Kusumaatmaja, H., Pooley, C.M., Girardo, S., Pisignano, D. and Yeomans, J.M., 2008. 'Capillary filling in patterned channels', *Physical Review E* 77(067301). DOI: 10.1103/PhysRevE.77.067301
- [32] Zhao, J., Chen, S. and Liu, Y., 2016. 'Droplets motion on chemically/topographically heterogeneous surfaces', *Molecular Simulation* 42, 1452-1459. DOI: 10.1080/08927022.2016.1198478
- [33] Kusumaatmaja, H., 2008. 'Lattice boltzmann studies of wetting and spreading on patterned surfaces', University of Oxford D. Phil. Thesis.
- [34] Zhang, J., Li, B. and Kwok, D.Y., 2009. 'Metastable contact angles and selfpropelled drop movement on chemically, heterogeneous surfaces by a meanfield lattice boltzmann model', *Eur. Phys. J. Special Topics* 171, 73-79. DOI: 10.1140/epjst/e2009-01013-y
- [35] Krüger, T., Kusumaatmaja, H., Kuzmin, A., Shardt, O., Silva, G. and Viggen, E.M., 2017a. The lattice Boltzmann method. Springer International Publishing, 10(978-3), pp.407-431.
- [36] Kendon, V.M., Cates, M.E., Pagonabarraga, I., Desplat, J.C. and Bladon, P., 2001. 'Inertial effects in three dimensional spinodal decomposition of a symmetric binary fluid

- mixture: a lattice boltzmann study', *J. Fluid Mech* 440, 147-203. DOI: 10.1017/S0022112001004682
- [37] Bray, A.J., 1994. 'Theory of phase-ordering kinetics', *Advances in Physics* 43(3), 357-459. DOI: 10.1080/00018739400101505
- [38] Swift, M.R., Orlandini, E., Osborn, W.R. and Yeomans, J.M., 1996. 'Lattice boltzmann simulations of liquid-gas and binary fluid systems', *Physical Review E* 54(5), 5041-5052. DOI: 10.1103/physreve.54.5041
- [39] Briant, A.J. and Yeomans, J.M., 2004. 'Lattice boltzmann simulations of contact line motion. ii. binary fluids', *Physical Review E* 69(031603). DOI: 10.1103/PhysRevE.69.031603
- [40] Krüger, T., Kusumaatmaja, H., Kuzmin, A., Shardt, O., Silva, G. and Viggen, E.M., 2017b. *The lattice Boltzmann method*. Springer International Publishing, 10(978-3), pp.65-66.
- [41] Bhatnagar, P.L., Gross, E.P. and Krook, M., 1954. 'A model for collision processes in gases. i. small amplitude processes in charged and neutral one component systems', *Physical Review* 94(3), 511-525. DOI: 10.1103/physrev.94.511
- [42] Pooley, C.M., Kusumaatmaja, H. and Yeomans, J.M., 2008. 'Contact line dynamics in binary lattice boltzmann simulations', *Physical Review E* 78(056709). DOI: 10.1103/PhysRevE.78.056709
- [43] Pooley, C.M., Kusumaatmaja, H. and Yeomans, J.M., 2009. 'Modelling capillary filling dynamics using lattice boltzmann simulations', *Eur. Phys. J. Special Topics* 171, 63-71. DOI: 10.1140/epjst/e2009-01012-0
- [44] Ladd, A., 1994. 'Numerical simulations of particulate suspensions via a discretized boltzmann equation. part 1. theoretical foundation', *Journal of Fluid Mechanics* 271, 285. DOI: 10.1017/s0022112094001771
- [45] Schrader, M., 1995. 'Young-dupre revisited', *Langmuir* 11, 3585-3589. DOI: 10.1021/la00009a049
- [46] Washburn, E. W., 1921. 'The dynamics of capillary flow', *The Physical Review* 17(3), 273. DOI: 10.1103/PhysRev.17.273
- [47] Cox, R., 1986. 'The dynamics of the spreading of liquids on a solid surface. part 1. viscous flow.', *Journal of Fluid Mechanics* 168(1), 169-194. DOI: 10.1017/s0022112086000332
- [48] Voinov, O., 1977. 'Hydrodynamics of wetting', *Fluid Dynamics* 11(5), 714-721. DOI: 10.1007/bf01012963
- [49] Latva-Kokko, M. and Rothman, D. H., 2007. 'Scaling of dynamic contact angles in a lattice-boltzmann model', *Physical Review Letters* 98(254503). DOI: 10.1103/PhysRevLett.98.254503
- [50] Teng, P., Tian, D., Fu, H. and Wang, S., 2020. 'Recent progress of electrowetting for droplet manipulation: from wetting to superwetting systems', *Mater. Chem. Front.* 4(140). DOI: 10.1039/c9qm00458k
- [51] Olanrewaju, A., Beaugrand, M., Yafia, M. and Juncker, D., 2018. 'Capillary microfluidics in microchannels: from microfluidic networks to capillary circuits', *Lab. Chip.* 18(16), 2323-2347. DOI: 10.1039/c8lc00458g
- [52] Mugele, F., Klingner, A., Buehrle, J., Steinhäuser, D. and Herminghaus, S., 2005. 'Electrowetting: a convenient way to switchable wettability patterns', *J. Phys.: Condens. Matter* 17, 559-576. DOI: 10.1088/0953-8984/17/9/016